Featured in Physics

Photon Pathways and the Nonperturbative Scaling Law of High Harmonic Generation

Mekha Vimal,[1] Martin Luttmann,[1] Titouan Gadeyne,[1,2] Matthieu Guer,[1] Romain Cazali,[1] David Bresteau,[1] Fabien Lepetit,[1] Olivier Tcherbakoff,[1] Jean-François Hergott,[1] Thierry Auguste,[1] and Thierry Ruchon[1,*]

[1]*Université Paris-Saclay, CEA, CNRS, LIDYL, 91191 Gif-sur-Yvette, France*

[2]*Département de Chimie, École Normale Supérieure, PSL University, 75005 Paris, France*

(Received 13 March 2023; revised 14 September 2023; accepted 3 October 2023; published 16 November 2023; corrected 11 July 2024)

High harmonic generation (HHG) has become a core pillar of attosecond science. Traditionally described with field-based models, HHG can also be viewed in a parametric picture, which predicts all properties of the emitted photons, but not the nonperturbative efficiency of the process. Driving HHG with two noncollinear beams and deriving analytically the corresponding yield scaling laws for any intensity ratio, we herein reconcile the two interpretations, introducing a generalized photonic description of HHG. It is in full agreement with field-based simulations and experimental data, opening the route to smart engineering of HHG with multiple driving beams.

DOI: 10.1103/PhysRevLett.131.203402

Attosecond science is currently building on evermore specialized light sources based on gas-phase high harmonic generation (HHG), an extremely nonlinear process in which an intense infrared laser is coherently up-converted into higher-order harmonics of its own frequency [1]. It provides extreme ultraviolet (XUV) or soft x-ray radiation [2–4] bunching as trains or isolated attosecond pulses, which can be utilized for the study of nuclear and electron dynamics with attosecond time resolution [5,6]. In addition, the ultrabroad coherent HHG spectrum carries information about the underlying dynamical nonlinear response of the medium on an attosecond timescale [4,7–9]. The current understanding of HHG relies on the solution of the time-dependent Schrödinger equation [10–15]. Upon simplifying assumptions, it leads to the strong field approximation (SFA). The latter directly matches the classical three-step model, wherein, driven by the laser electric field, an outermost electron of the atom is tunnel ionized, accelerated in the continuum, and finally recombined with the ionic core, emitting its excess of energy as an XUV photon [16–19]. All three steps depend nonlinearly on the exact waveform of the driving field [18,20]. Nevertheless, HHG in a gas jet can be approximated using a simple empirical treatment often referred to as the thin-slab model (TSM) [21,22], or active grating model [23]. Neglecting longitudinal phase-matching effects, HHG is approximated as happening in a single plane, in which the electric field of harmonic q scales as $|E|^{q_{\mathrm{eff}}}$, and has a phase $q\arg[E]+\alpha_{\mathrm{at}}|E|^2$, where E is the electric field of the driving laser, and q_{eff} and α_{at} being two constants depending on the species and wavelength. This model has been extremely successful in a great variety of experimental conditions [24–26]. Importantly, $q_{\mathrm{eff}} \neq q$ reflects the nonperturbative nature of HHG: Although the properties (energy, linear, and angular momenta) of the harmonic photons can be perfectly understood as originating from the addition of q photons from the driving field, the harmonic yield does not scale as $|E|^q$ as in perturbative nonlinear optics phenomena [27]. Indeed, one of the most distinctive feature of HHG is the formation of a spectral plateau, over which the efficiency varies moderately with the harmonic order.

A special case of HHG which has drawn increasing attention in both fundamental studies and applications is the so-called noncollinear HHG (NCHHG), wherein two beams crossing with an angle at focus are used. In this geometry, each harmonic is angularly split into several beamlets [21,28,29], whose properties can be different and finely controlled by modifying the two driving beams. For instance, beamlets with varying spin [30,31] and orbital [32,33] angular momenta were observed, opening the road to applications [34,35]. The properties of each beamlet can be easily understood within the parametric picture: Conservation laws require that a photon in beamlet p of harmonic q results from the absorption of $(q-p)$ photons from the first beam, and p from the second, summing their momenta and energies. Although the photon picture fails to predict the general nonperturbative yield of HHG, Bertrand *et al.* [29] have shown experimentally that in the case of NCHHG with a very weak secondary beam, the intensity of beamlet p obeys a perturbative scaling law $I_p \propto (I_2)^p$, with I_2 the intensity of the second beam. This yield law was later refined by Li *et al.* [36] using a quantum optical model to describe the saturation observed as the intensity in the secondary beam is increased. These descriptions, however, remain limited to a narrow range of intensity ratios: As soon as the yields start to deviate from the perturbative behavior, the exact form of the yield law is no longer known, and the intuitive interpretation in terms of perturbative photon channels is lost. It is puzzling

that the photon model is able to predict the yield of individual beamlets in NCHHG over a narrow range of intensities, but fails beyond or in regular collinear HHG, while still predicting other properties of the harmonic beams in all these situations. This asks for more experimental investigations of the yield laws in NCHHG, which are fairly scarce to date, and for a unifying framework that could conciliate both field-based and photon-based approaches.

In this Letter, we use an analytical expansion of the TSM to derive the yield laws of NCHHG beamlets for any intensity ratio of the two beams. We are able to readily interpret the form of these laws in terms of competing photon channels, in full compatibility with previous interpretations. We compare this model to experiments covering the complete range of ratios, and to numerical simulations based on the SFA including phase matching. This paper is accompanied by a joint publication [37], in which we demonstrate that the scaling laws derived here can be visually deduced from the spatial profile of the harmonic beamlets when driving NCHHG with structured beams.

The experimental setup is based on a Ti:sapphire femtosecond laser, which delivers pulses of 1.5 mJ energy, 25 fs FWHM duration, at a repetition rate of 1 kHz [38]. The beam is split into two using an optical beam splitter. The main beam carries enough energy to generate harmonics on its own when focused by a 75 cm focal length lens, with a cutoff about harmonic 19 corresponding to an intensity of $\sim 0.5 \times 10^{14}$ W/cm^2. The second beam passes through a motorized adjustable attenuator enabling the adjustment of its amplitude before being focused by an identical lens. We define α as $|E_2/E_1|$, the ratio of the amplitudes of the two beams at focus. The two beams are temporally overlapped and cross at an adjustable angle at focus, in a jet of argon gas [Fig. 1(a)]. The experimental parameters are optimized for short trajectories by adjusting the focusing lens position and irises [39]. The generated harmonics are then detected by a photon spectrometer based on a grating and microchannel plates equipped with a phosphor screen, finally imaged on a CCD camera.

Figures 1(b) and 1(c) show typical images recorded by the camera for different levels of perturbation, showing the expected series of beamlets for each harmonic order. We observe nicely round-shaped beamlets, with a cutoff about harmonic 19, which agrees with the peak intensity estimation, and rules out important plasma-induced effects. As established in Refs. [21,29,40], the wave vector associated with the pth beamlet ($p = 0$ where $\theta_x = 0$), for harmonic q, is given by $\vec{k}_{q,p} = (q-p)\vec{k}_1 + p\vec{k}_2$, where $\vec{k}_1$ and $\vec{k}_2$ are the wave vectors associated with each beam. For large α, the $p \geq 0$ side is clearly dominating, and the first beamlets $p = 0$, 1, 2 start to fade out.

Being able to finely scan the amplitude ratio of the two beams, we first explored a narrow range of α close to $\alpha = 0$ to observe a perturbative behavior with respect to beam 2. The intensity I_1 was fixed while I_2 was varied such that α

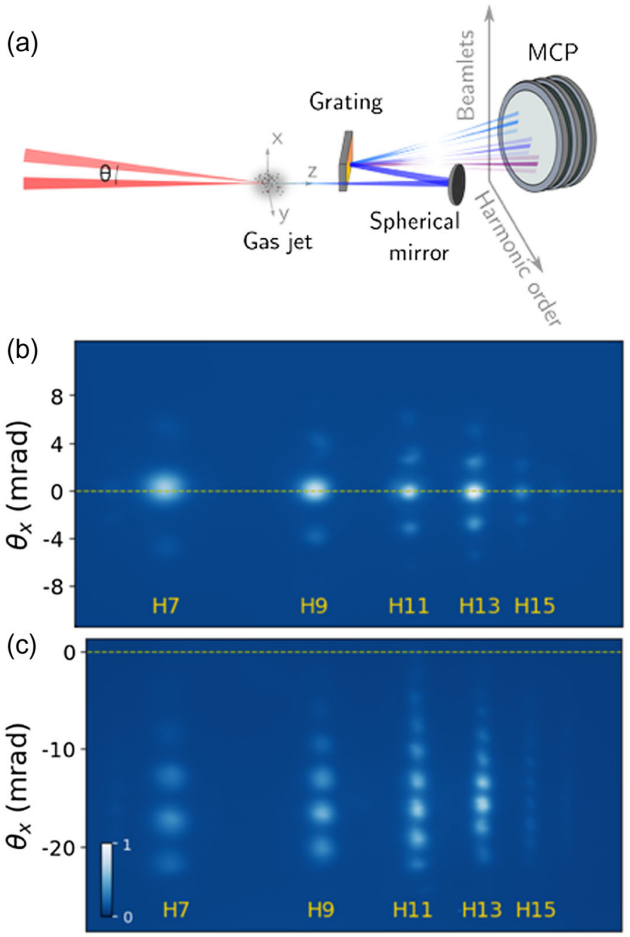

FIG. 1. (a) Schematic of the experimental setup. θ is in the x-z plane. At the bottom are typical images observed on the microchannel plate (x-y plane) for (b) low ($\alpha \ll 1$) and (c) high ($\alpha \approx 1$) perturbation regimes. The dashed yellow line marks the position of the zeroth order of diffraction, i.e., the position of the spectrum generated by beam 1 alone. The angle between the driving beams is respectively 40 mrad (b) and 28 mrad (c).

spanned from 0 to 0.15, allowing us to observe beamlets up to $p = 2$. The intensity of each beamlet was summed over a constant-sized box centered on its peak. Basic processing (Supplemental Material S2 [41]) yields the magnitude of the electric field $|E_q^p|$ displayed in Fig. 2(a) as a function of α. The fits with the perturbative scaling law $|E_q^p| \propto \alpha^{|p|}$ are indicated as dot-dashed lines. The trends are the same for all harmonics (Supplemental Material S2 [41]). We observe that the fit is only acceptable up to $\alpha = 0.05$, above which experimental yields progressively depart from this law, and we note a saturation followed by a decrease.

To understand these observations, we perform an analytical development of the TSM. We consider two laser beams, one propagating in the x-z plane linearly polarized along x, with wave vector $\vec{k}_1$ and the other with $\vec{k}_2$ forming a small angle θ with the first beam and linearly polarized in the x-z plane. Although this polarization configuration

creates a small longitudinal field, and is not ideal for interferences, it is experimentally favorable for the optics used, and we have chosen it. In the following, we neglect the (weak) longitudinal field along z. We write $\Delta\vec{k} = \vec{k}_1 - \vec{k}_2$ and $\Delta k^{\perp}$ the projection of $\Delta\vec{k}$ along the transverse x direction. The electric field at location $\vec{r}$ reads

$$E(\vec{r}) = E_0 e^{-i\vec{k}_1\cdot\vec{r}}\left(1 + \alpha e^{i\Delta\vec{k}\cdot\vec{r}}\right). \tag{1}$$

In the TSM, we estimate the field of harmonic q as

$$E_q^{\mathrm{NF}} \propto |E|^{q_{\mathrm{eff}}} e^{i(q\arg[E]+\varphi_{\mathrm{at}})} = (E)^{q^+}(E^*)^{q^-} e^{i\varphi_{\mathrm{at}}} \tag{2}$$

with $q_{\mathrm{eff}} \simeq 3.5$ for our experimental conditions [22,42], $q^{\pm} = (q_{\mathrm{eff}} \pm q)/2$, and $\varphi_{\mathrm{at}} \simeq \alpha_{\mathrm{at}}|E|^2$ is the atomic phase. Neglecting the latter (see Supplemental Material S1 [41] for a brief description, which includes Refs. [43,44]), we apply the generalized binomial theorem with ascending powers on α to get, for $\alpha < 1$,

$$E_q^{\mathrm{NF}} \propto |E_0|^{q_{\mathrm{eff}}} e^{iq\arg[E_0]} \sum_{p=-\infty}^{+\infty} e^{ip\Delta k^{\perp}x} \sum_{n=0}^{+\infty} \alpha^{|p|+2n} a_p^n$$

$$\text{with} \qquad a_p^n = \binom{q^+}{n+\frac{|p|+p}{2}} \binom{q^-}{n+\frac{|p|-p}{2}}. \tag{3}$$

The a_p^n coefficients are products of two generalized binomial coefficients. They stem from the expansions of $(E)^{q^+}$ and $(E^*)^{q^-}$ in Eq. (2), which may be associated, respectively, with absorption and stimulated emission photonic processes driven by the composite field. Upon Fourier transform to the far field, Eq. (3) yields a beamlet for every relative integer p, spreading along the x axis. For reaching beamlet p, the leading term in the expansion $n = 0$ corresponds to the absorption (or emission for $p < 0$) of $|p|$ photons in the composite beam, scaling perturbatively as $\alpha^{|p|}$, as already inferred in Refs. [29,36]. With α increasing, we predict an infinite number of additional contributions scaling as $\alpha^{|p|+2n}$. We notice that the exponents in this series are the same as those obtained by expanding the nonlinear polarization induced by a sum of two fields in the general case [45]. Following this, we interpret the higher-order terms as competing photon pathways, in which n additional pairs of photons are simultaneously absorbed and emitted [see Fig. 2(c)]. For a given p, all pathways with $n \neq 0$ end up on the same energy level and with the same $\vec{k}_{q,p}$ wave vector as the $n = 0$ one, all adding up coherently and altering the beamlet yield scaling law. The a_p^n coefficients are the weights of the corresponding photon pathways and are fairly intuitive to compute: In their expression $n + [(|p| + p)/2]$ (resp., $n + [(|p| - p)/2]$) is simply the total number of photons absorbed (resp., emitted) in the secondary beam.

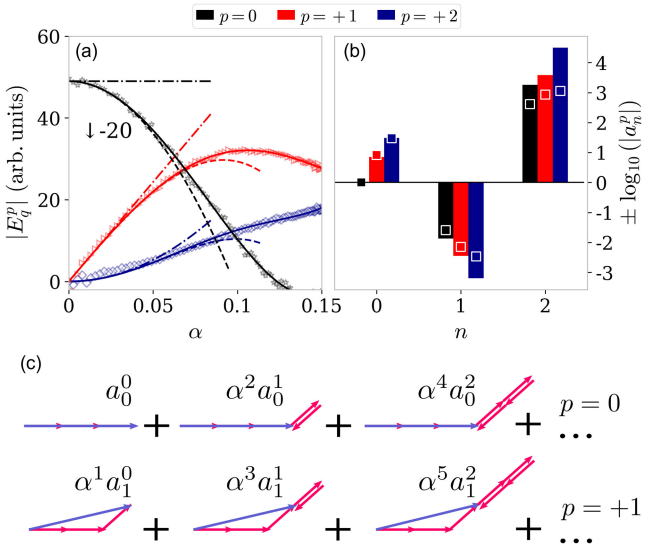

FIG. 2. (a) Experimental amplitude of the electric fields of beamlets $p = 0$, $+1$, and $+2$ for harmonic $q = 13$. These curves are fitted with one (dot-dashed), two (dashed lines), or three (solid lines) terms of Eq. (4). (b) Comparing the experimental fit coefficients (filled bars) to the analytical a_p^n coefficients (square markers, signs were adjusted to have the first coefficient be positive). The signs of the first few successive coefficients are seen to alternate. (c) Illustration of the photon pathways contributing to beamlets $p = 0$ and 1, for $q = 3$.

The field of beamlet p for harmonic q in the far field therefore scales as

$$E_q^p \propto a_p^0 \alpha^{|p|} + a_p^1 \alpha^{|p|+2} + a_p^2 \alpha^{|p|+4} + \ldots \tag{4}$$

From this generalized scaling law, we predict that the terms in higher powers of the perturbation are of the same parity as the leading one. In the companion paper [37], we demonstrate that this property is directly imprinted on the parity of the transverse profile of the beamlets when driving NCHHG with structured beams.

To test this scaling law, we fit the experimental yields of Fig. 2(a) with an increasing number of terms (see Supplemental Material S2 [41] for other harmonic orders). The dot-dashed lines are obtained with the leading term only (as already mentioned above), the dashed lines with two, and the solid lines with three, of the expected parity. The fit function with three terms is excellent for all sets of data over this α range. Inspecting the coefficients of expansion obtained by fitting [Fig. 2(b)], we observe satisfactory agreement with the analytical values, featuring a progressive increase of their magnitude with n and, strikingly, alternating signs. Interestingly, this alternation in sign implies that the absorption and subsequent emission of a photon dephases the harmonic emission by π. This is very reminiscent of the phase difference between adjacent sidebands in RABBITT [46], or the phase between harmonics in ATI [47,48]. Furthermore, this result could fuel

the current discussion about the phase of stimulated emission [49].

We further tested our analytical model by extending the experiment to a broader range of α values, reaching up to $\alpha = 1$ for which the two beams have equal intensities. We report in Fig. 3(a) the experimental yields of each beamlet of harmonic $q = 15$ against α (see Supplemental Material S3 [41] for other harmonic orders). Again, we kept the intensity of the main beam constant and increased that of the second beam. Even though the total intensity increases with α, each beamlet reaches a maximum at a given value of α, and eventually fades out. We compared this behavior to full numerical simulations based on the solution of the nonadiabatic, three-dimensional paraxial wave equation (PWE) performed in Cartesian geometry, in which the source term in the PWE is given by the solution of the Schrödinger equation in the SFA. The results of this model, valid for high enough harmonic orders, are displayed in Fig. 3(b) for harmonic $q = 15$. We find excellent agreement with the experimental result. Finally, we computed the yields analytically with Eq. (3), limiting it to $n \leq 15$ [Fig. 3(c)]. The agreement is remarkably good for such a simple model. As highlighted in the insets for $p = 1$, the general shape of the yield as a function of α is nicely reproduced, including the main Gaussian-like peak followed by a smaller secondary peak. These unexpected secondary maxima tend to fade out for higher p in the experiment, numerical, and analytical models. Our interpretation of HHG in terms of interfering photon pathways perfectly suits these observations: As the intensity of the second beam increases, more and more photon pathways contribute to the total yield, and since successive channels are essentially π out of phase, they may form interference structures. When there are just a few contributing pathways (that is, for low-p beamlets that are bright near $\alpha = 0$), these interferences result in sharp and identifiable secondary peaks.

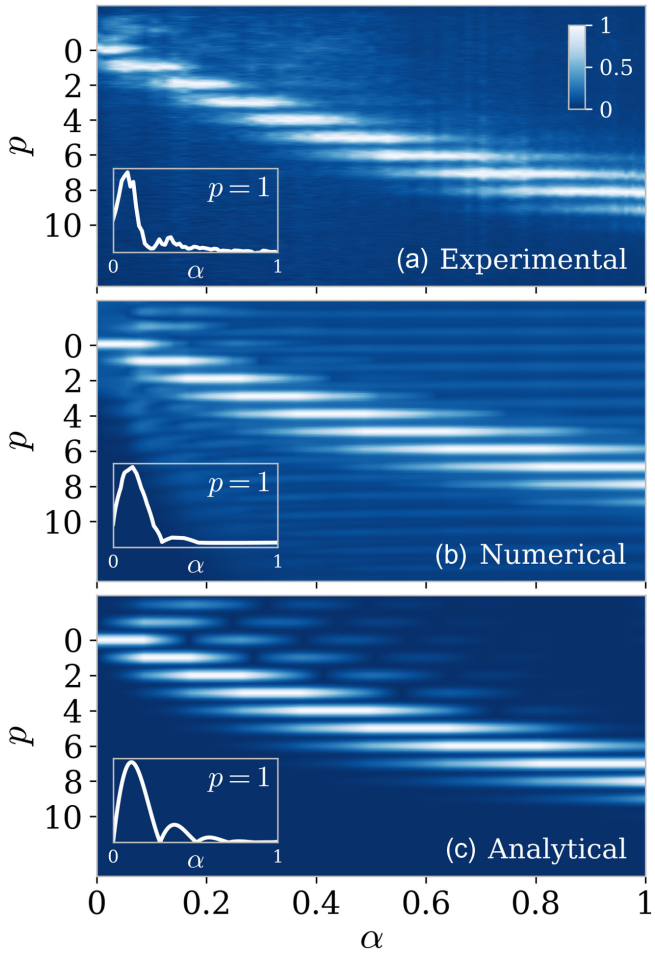

FIG. 3. Experimental (a), numerical (SFA) (b), and analytical (c) field amplitude of the beamlets of harmonic $q = 15$ as a function of the amplitude ratio α of the two driving beams. The amplitudes were normalized by the maximum for each column to optimize readability over the whole α range. For the analytical plot, values of n up to 15 were used in Eq. (3). The insets in the corners are lineouts of the field amplitude of order $p = 1$ normalized to take into account the changing total field intensity as α is increased.

Taking our analytical development in the collinear limit $\Delta k^{\perp} \to 0$, all p terms in Eq. (3) are summed to form the harmonic field, and we recover a series of α^m terms with coefficients $\binom{q_{\text{eff}}}{m}$, as expected from directly applying the binomial theorem to the collinear case (Supplemental Material S1 [41]). However, the direct interpretation of this series in terms of photonic processes is much less straightforward, as all channels add up to form a single harmonic beam. Through our noncollinear geometry, we could identify the photon pathways underlying this formula, in a way that is consistent with the observations that the properties of beamlet p result from the net absorption of p photons from the secondary beam. One may ask why, in our extended parametric picture, extra photons only seem to be exchanged with beam 2 [Fig. 2(c)]. In fact, the additional pathways involving photons from beam 1 are hidden in the global $|E_0|^{q_{\text{eff}}}$ factor in Eq. (3), which effectively describes single-beam HHG and thus cannot, as we have seen, be trivially rewritten as a sum of photon pathways. In this work, adding a second beam and factorizing out the single-beam physics was the key to revealing yield laws that suggest a photon-based explanation to the nonperturbative efficiency of HHG.

We note that our results would have been very different for a perturbative $q_{\text{eff}} = q$ power law, in which case $q^- = 0$ and Eq. (3) reduces to a single sum, such that a single photonic process scaling as α^p contributes to beamlet p. Investigating the yields of HHG in a noncollinear scheme thus unveils the multiple pathways that interfere with one another and govern the nonperturbative yield of HHG. Negative p beamlets, which involve stimulated emission of photons, would also be missing if the physics of HHG was perturbative (Supplemental Material S1 [41]). Furthermore,

it should be noted that the value of q_{eff} rules the thickness and width of the yield curves (Supplemental Material S1 [41]), which could give an access door to the precise determination of its experimental value.

In conclusion, with an analytical development of the thin-slab model and extensive experimental data, we were able to bridge the gap between field-based and photon-based interpretations of NCHHG for any intensity ratio of the beams. Our analysis unveiled, contrary to previous interpretations, that successive higher-order terms involving a series of absorption and stimulated emission of photon pairs play the main role, leading to polynomial yield laws with exponents of given parities, giving rise to an unexpectedly rich structure of secondary maxima in the beamlet yields. This photon-pathway formalism is reminiscent of Feynman diagrams in quantum field theory. It renews our parametric understanding of HHG, as a coherent combination of several "higher than qth-order" photon channels. We note that such approaches were earlier promoted for perturbative nonlinear optics [50–52], though never unveiled experimentally in HHG. We also note that a consistent quantum field theory of HHG should be able to retrieve the a_p^n coefficients of Eq. (3) for the amplitude of each photon pathway.

These results set a reference framework for the design of new HHG-based attosecond sources in noncollinear geometry, whether they be in cavities or not. Even though the experimental results presented here are for two Gaussian beams with the same central wavelength, the same model could also be applied to cases in which beams have different spatial profiles (carrying orbital angular momentum, for instance), as well as different wavelengths. They could also be used to reexamine NCHHG experiments with smaller crossing angles, casting new light on the interpretation of the results in relation to the perturbation levels [8,53–56]. Also, we have not exploited the results to get insights into the spectroscopic peculiarities of the processes, but it has the prospect of becoming a unique analysis tool. Finally, it should be noted that we have deliberately ignored phase-matching effects [31,57,58] that should be included in future work. As a first extension, in the companion paper [37], we examine the case of two spatially structured driving beams, which highlights in a very visual way the transition from perturbative to nonperturbative scaling laws in NCHHG.

The authors thank C. Hernández-García and L. Plaja for helpful discussion. The authors gratefully acknowledge Yann Mairesse from CELIA Bordeaux for lending a spectrometer. This work is supported by the French "Investments for the Future" program of the Agence Nationale pour la Recherche (Contracts No. 11-EQPX0005-ATTOLAB and ANR HELIMAG ANR-21-CE30-0037), LabEx PALM (Grant No. ANR-10-LABX-0039-PALM) through the Atto-FOAM project, the Scientific Cooperation Foundation of Paris-Saclay University through the OPT2X project (Grant No. Lidex OPT2X-2014), by the Île-de-France region through the Pulse-X project, and by the European Union's Horizon 2020 Research and Innovation Programme, Grant No. EU-H2020-LASERLAB-EUROPE-654148. The École Normale Supérieure is gratefully acknowledged for T. G.'s fellowship.

*thierry.ruchon@cea.fr

[1] J. Biegert, F. Calegari, N. Dudovich, F. Quéré, and M. Vrakking, J. Phys. B **54**, 070201 (2021).
[2] M. Ferray, A. L'Huillier, X. F. Li, G. Mainfray, and C. Manus, J. Phys. B **21**, L31 (1988).
[3] X. F. Li, A. L'Huillier, M. Ferray, L. A. Lompre, and G. Mainfray, Phys. Rev. A **39**, 5751 (1989).
[4] J. Li, J. Lu, A. Chew, S. Han, J. Li, Y. Wu, H. Wang, S. Ghimire, and Z. Chang, Nat. Commun. **11**, 2748 (2020).
[5] F. Calegari, G. Sansone, S. Stagira, C. Vozzi, and M. Nisoli, J. Phys. B **49**, 062001 (2016).
[6] L. Gallmann, I. Jordan, H. J. Wörner, L. Castiglioni, M. Hengsberger, J. Osterwalder, C. A. Arrell, M. Chergui, E. Liberatore, U. Rothlisberger, and U. Keller, Struct. Dyn. **4**, 061502 (2017).
[7] O. Pedatzur, G. Orenstein, V. Serbinenko, H. Soifer, B. D. Bruner, A. J. Uzan, D. S. Brambila, A. G. Harvey, L. Torlina, F. Morales, O. Smirnova, and N. Dudovich, Nat. Phys. **11**, 815 (2015).
[8] K.-Y. Chang, L.-C. Huang, K. Asaga, M.-S. Tsai, L. Rego, P.-C. Huang, H. Mashiko, K. Oguri, C. Hernández-García, and M.-C. Chen, Optica **8**, 484 (2021).
[9] A. Camper, E. Skantzakis, R. Géneaux, F. Risoud, E. English, Z. Diveki, N. Lin, V. Gruson, T. Auguste, B. Carré, R. R. Lucchese, A. Maquet, R. Taïeb, J. Caillat, T. Ruchon, and P. Salières, Optica **8**, 308 (2021).
[10] K. C. Kulander and B. W. Shore, Phys. Rev. Lett. **62**, 524 (1989).
[11] J. H. Eberly, Q. Su, and J. Javanainen, Phys. Rev. Lett. **62**, 881 (1989).
[12] J. L. Krause, K. J. Schafer, and K. C. Kulander, Phys. Rev. Lett. **68**, 3535 (1992).
[13] V. C. Reed and K. Burnett, Phys. Rev. A **46**, 424 (1992).
[14] M. Lewenstein, P. Balcou, M. Y. Ivanov, A. L'Huillier, and P. B. Corkum, Phys. Rev. A **49**, 2117 (1994).
[15] L. Gao, X. Li, P. Fu, R. R. Freeman, and D.-S. Guo, Phys. Rev. A **61**, 063407 (2000).
[16] K. C. Kulander, K. J. Schafer, and J. L. Krause, in *Super-Intense Laser-Atom Physics*, edited by B. Piraux, A. L'Huillier, and K. Rzazewski (Springer US, Boston, 1993), pp. 95–110.
[17] P. B. Corkum, Phys. Rev. Lett. **71**, 1994 (1993).
[18] O. Smirnova and M. Ivanov, in *Attosecond and XUV Physics* (Wiley-VCH Verlag GmbH & Co. KGaA, New York, 2014), pp. 201–256.
[19] K. Amini *et al.*, Rep. Prog. Phys. **82**, 116001 (2019).
[20] A.-T. Le, R. R. Lucchese, S. Tonzani, T. Morishita, and C. D. Lin, Phys. Rev. A **80**, 013401 (2009).
[21] Y. Mairesse, N. Dudovich, J. Levesque, D. Kartashov, D. M. Villeneuve, P. B. Corkum, and T. Auguste, Opt. Lett. **32**, 436 (2007).

[22] L. Rego, J. S. Román, L. Plaja, A. Picón, and C. Hernández-García, *Vortex Dynamics and Optical Vortices* (IntechOpen, Rijeka, Croatia, 2017).
[23] C. Chappuis, D. Bresteau, T. Auguste, O. Gobert, and T. Ruchon, Phys. Rev. A **99**, 033806 (2019).
[24] C. Hernández-García, J. S. Román, L. Plaja, and A. Picón, New J. Phys. **17**, 093029 (2015).
[25] L. Rego, J. S. Román, A. Picón, L. Plaja, and C. Hernández-García, Phys. Rev. Lett. **117**, 163202 (2016).
[26] A. I. Gonzalez, G. Jargot, P. Rigaud, L. Lavenu, F. Guichard, A. Comby, T. Auguste, O. Sublemontier, M. Bougeard, Y. Zaouter, P. Georges, M. Hanna, and T. Ruchon, J. Opt. Soc. Am. B **35**, A6 (2018).
[27] R. W. Boyd, *Nonlinear Optics*, 3rd ed. (Academic, New York, 2008).
[28] A. V. Birulin, V. T. Platonenko, and V. V. Strelkov, Quantum Electron. **26**, 377 (1996).
[29] J. B. Bertrand, H. J. Wörner, H.-C. Bandulet, É. Bisson, M. Spanner, J.-C. Kieffer, D. M. Villeneuve, and P. B. Corkum, Phys. Rev. Lett. **106**, 023001 (2011).
[30] D. D. Hickstein, F. J. Dollar, P. Grychtol, J. L. Ellis, R. Knut, C. Hernández-García, D. Zusin, C. Gentry, J. M. Shaw, T. Fan, K. M. Dorney, A. Becker, A. Jaroń-Becker, H. C. Kapteyn, M. M. Murnane, and C. G. Durfee, Nat. Photonics **9**, 743 (2015).
[31] J. L. Ellis, K. M. Dorney, C. G. Durfee, C. Hernández-García, F. Dollar, C. A. Mancuso, T. Fan, D. Zusin, C. Gentry, P. Grychtol, H. C. Kapteyn, M. M. Murnane, and D. D. Hickstein, Opt. Express **25**, 10126 (2017).
[32] D. Gauthier, P. R. Ribič, G. Adhikary, A. Camper, C. Chappuis, R. Cucini, L. F. DiMauro, G. Dovillaire, F. Frassetto, R. Géneaux, P. Miotti, L. Poletto, B. Ressel, C. Spezzani, M. Stupar, T. Ruchon, and G. D. Ninno, Nat. Commun. **8**, 14971 (2017).
[33] F. Kong, C. Zhang, F. Bouchard, Z. Li, G. G. Brown, D. H. Ko, T. J. Hammond, L. Arissian, R. W. Boyd, E. Karimi, and P. B. Corkum, Nat. Commun. **8**, 14970 (2017).
[34] O. Neufeld, D. Ayuso, P. Decleva, M. Y. Ivanov, O. Smirnova, and O. Cohen, Phys. Rev. X **9**, 031002 (2019).
[35] M. Fanciulli, D. Bresteau, M. Vimal, M. Luttmann, M. Sacchi, and T. Ruchon, Phys. Rev. A **103**, 013501 (2021).
[36] L. Li, P. Lan, L. He, X. Zhu, J. Chen, and P. Lu, Phys. Rev. Lett. **120**, 223203 (2018).
[37] M. Luttman, M. Vimal, M. Guer, T. Gadeyne, C. Chappuis, J.-F. Hergott, and T. Ruchon, companion paper, Phys. Rev. A **108**, 053509 (2023).
[38] A. Golinelli, X. Chen, B. Bussière, E. Gontier, P.-M. Paul, O. Tcherbakoff, P. D'Oliveira, and J.-F. Hergott, Opt. Express **27**, 13624 (2019).
[39] P. Balcou, P. Salieres, A. L'Huillier, and M. Lewenstein, Phys. Rev. A **55**, 3204 (1997).
[40] G. Shoulga and A. Bahabad, Phys. Rev. A **99**, 043813 (2019).
[41] See Supplemental Material at http://link.aps.org/supplemental/10.1103/PhysRevLett.131.203402 for details on the binomial expansion of the electric field, results of the full-quantum model simulation and details pertaining to the processing of the experimental data.
[42] C. G. Wahlström, J. Larsson, A. Persson, T. Starczewski, S. Svanberg, P. Salieres, P. Balcou, and A. L'Huillier, Phys. Rev. A **48**, 4709 (1993).
[43] F. Catoire, A. Ferré, O. Hort, A. Dubrouil, L. Quintard, D. Descamps, S. Petit, F. Burgy, E. Mével, Y. Mairesse *et al.*, Phys. Rev. A **94**, 063401 (2016).
[44] K. Varjù, Y. Mairesse, B. Carré, M. Gaarde, P. Johnsson, S. Kazamias, R. Lopez-Martens, J. Mauritsson, K. Schafer, P. Balcou, A. L'Huillier, and P. Salières, J. Mod. Opt. **52**, 379 (2005).
[45] V. V. Strelkov, Phys. Rev. A **93**, 053812 (2016).
[46] D. Bharti, D. Atri-Schuller, G. Menning, K. R. Hamilton, R. Moshammer, T. Pfeifer, N. Douguet, K. Bartschat, and A. Harth, Phys. Rev. A **103**, 022834 (2021).
[47] L. J. Zipp, A. Natan, and P. H. Bucksbaum, Optica **1**, 361 (2014).
[48] M. Bertolino and J. M. Dahlström, Phys. Rev. Res. **3**, 013270 (2021).
[49] M. Pollnau, Optica **5**, 465 (2018).
[50] J. F. Ward, Rev. Mod. Phys. **37**, 1 (1965).
[51] N. L. Manakov and V. D. Ovsyannikov, Sov. J. Exp. Theor. Phys. **52**, 895 (1980).
[52] L. Pan, K. T. Taylor, and C. W. Clark, J. Opt. Soc. Am. B **7**, 509 (1990).
[53] K. T. Kim, C. Zhang, A. D. Shiner, B. E. Schmidt, F. Légaré, D. M. Villeneuve, and P. B. Corkum, Nat. Photonics **7**, 958 (2013).
[54] M. Louisy, C. L. Arnold, M. Miranda, E. W. Larsen, S. N. Bengtsson, D. Kroon, M. Kotur, D. Guénot, L. Rading, P. Rudawski, F. Brizuela, F. Campi, B. Kim, A. Jarnac, A. Houard, J. Mauritsson, P. Johnsson, A. L'Huillier, and C. M. Heyl, Optica **2**, 563 (2015).
[55] K. T. Kim, K. Kim, and T. J. Hammond, J. Phys. B **50**, 024002 (2017).
[56] S. Bengtsson and J. Mauritsson, J. Phys. B **52**, 063002 (2019).
[57] C. M. Heyl, P. Rudawski, F. Brizuela, S. N. Bengtsson, J. Mauritsson, and A. L'Huillier, Phys. Rev. Lett. **112**, 143902 (2014).
[58] K. A. Tran, K. B. Dinh, P. Hannaford, and L. V. Dao, J. Appl. Phys. **124**, 015901 (2018).

Correction: The previously published Fig. 1 had errors in the vertical scales of panels (a) and (b) and in the corresponding caption. The figure has been replaced and the last sentence of the caption has been modified accordingly.